# Supplementary Information

## Structural stability changes of the Atlantic Meridional Overturning Circulation

**Mihai Dima[1,2]*, Gerrit Lohman[2], Denis Nichita[1,2], Gregor Knorr[2] and Patrick Scholtz[2]**

[1]University of Bucharest, Faculty of Physics

[2]Alfred Wegener Institute for Polar and Marine Research

### Content

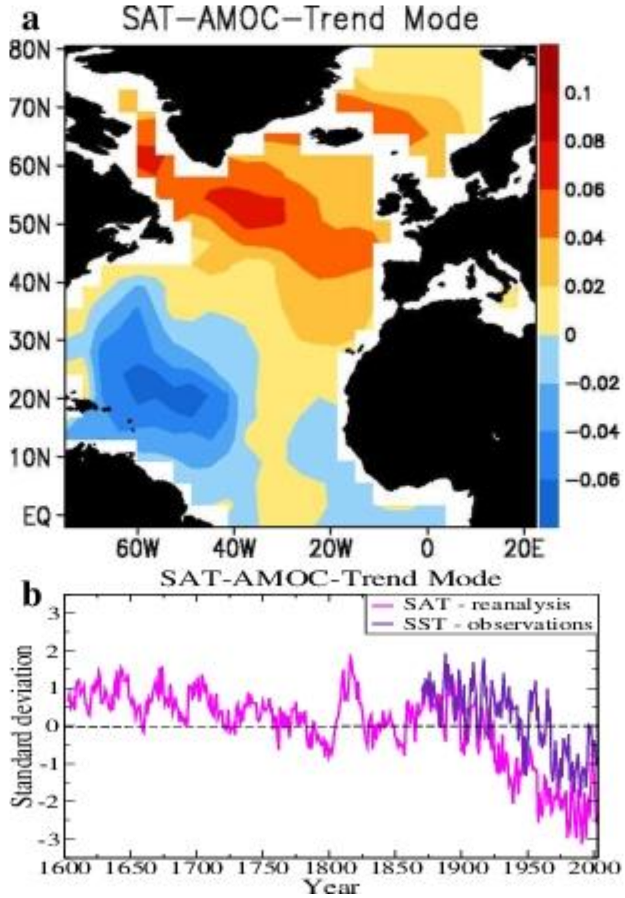


**Supplementary Figure 1 The SST-AMOC-Trend Mode identified in the multi-century reanalysis SAT fields.** a) The dominant mode identified through EOF analysis of the SAT fields extending over the 1603-2003 period; b) the time component of the dominant mode (magenta line) and the time series of the SST-AMOC-TM (violet line) identified through EOF analysis of the observed SST fields (Fig. 1c).

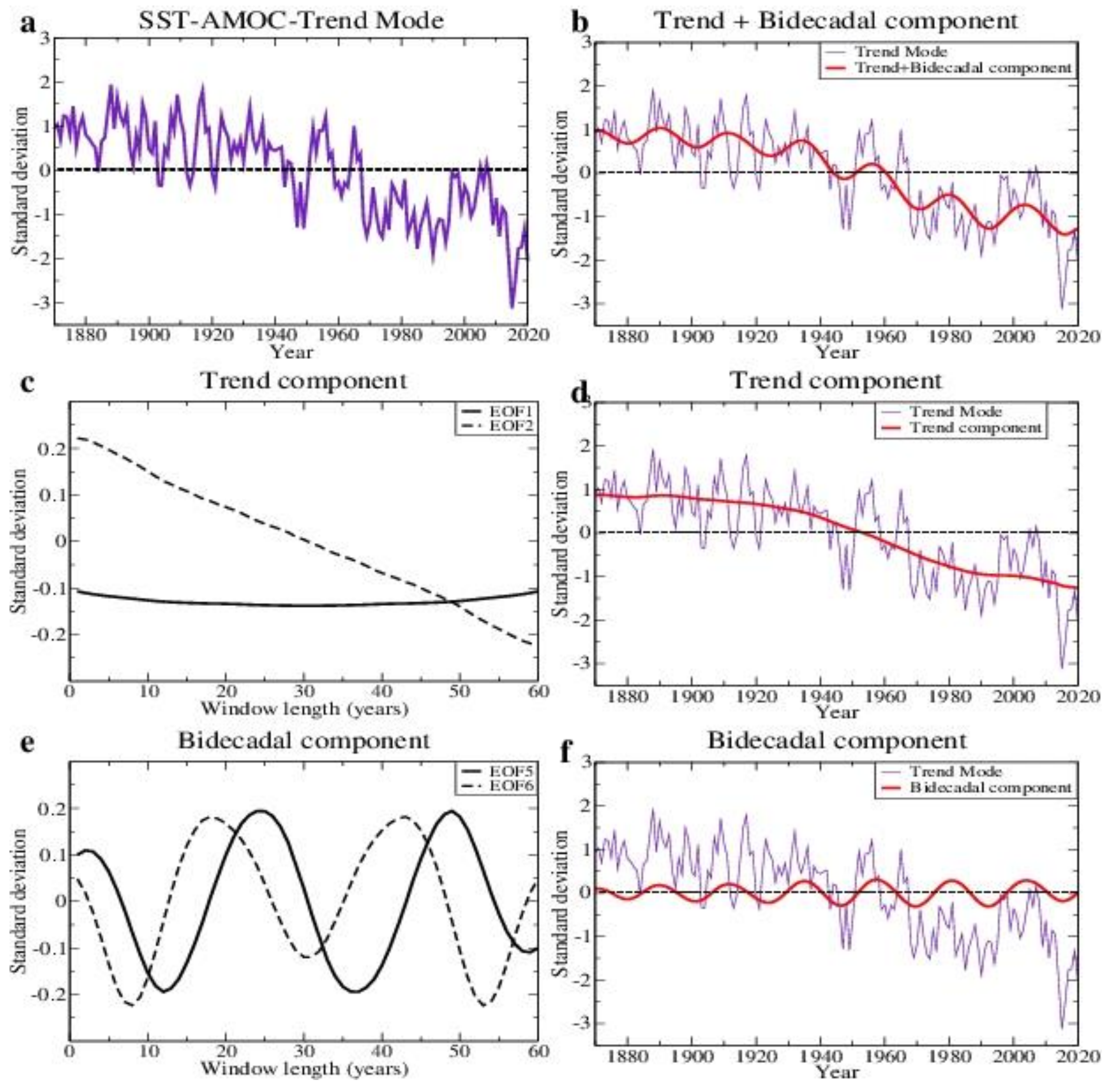


**Supplementary Figure 2 Singular Spectrum Analysis of the time component of SST-TM.** a) SST-AMOC-TM time component; b) reconstruction based on the long-term component and of the bidecadal oscillation; c) Time-EOFs associated with the centennial scale component; d) reconstructed centennial scale component; e) Time-EOFs associated with the bidecadal component; f) reconstructed bidecadal component. A 60-year window is used in the SSA.

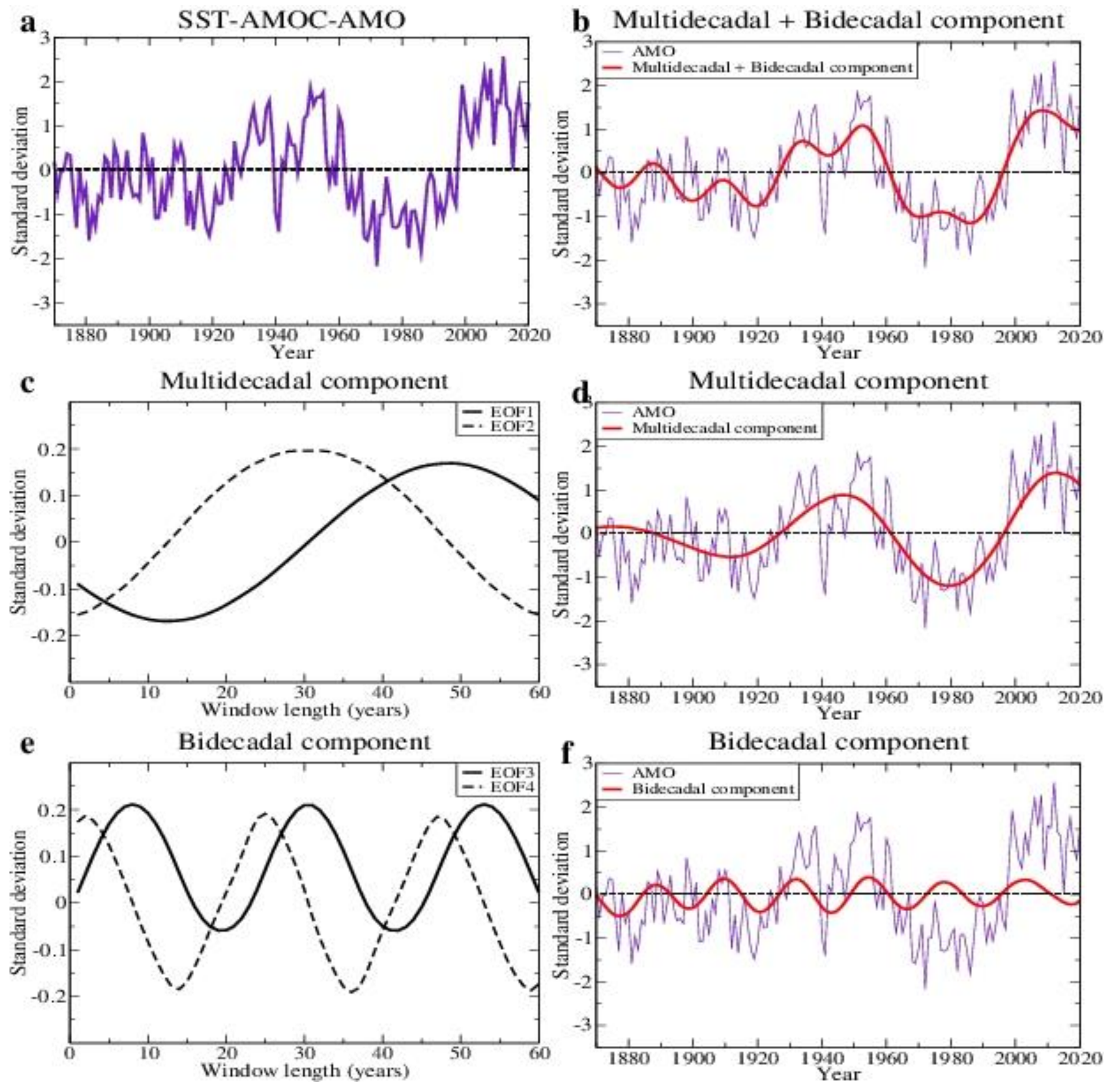


**Supplementary Figure 3 Singular Spectrum Analysis of the time component of SST-AMO.** a) SST-AMOC-AMO time component; b) reconstruction based on the multidecadal and the bidecadal oscillations; c) Time-EOFs associated with the multidecadal component; d) reconstructed multidecadal oscillation; e) Time-EOFs associated with the bidecadal oscillation; f) reconstructed bidecadal oscillation. A 60-year window is used in the SSA.

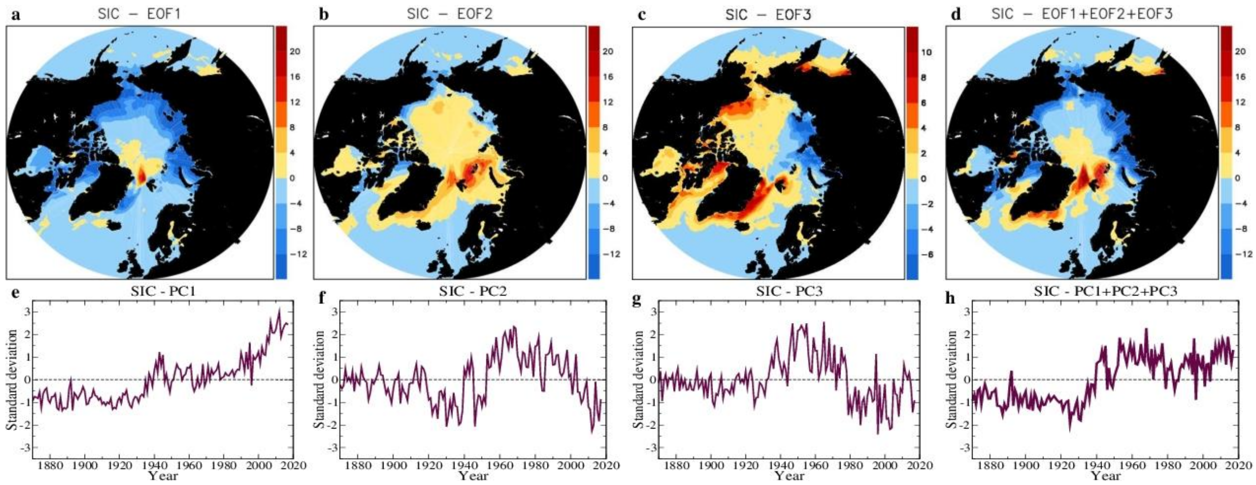


**Supplementary Figure 4 Deriving a freshwater forcing index related to SIC changes.** First three dominant JJAS SIC modes derived through EOF analysis. a) the dominant SIC mode, explaining 35% of variance; b) the second dominant mode, explaining 10% of variance; c) the third SIC mode, explaining 10% of variance; d) the superposition of EOF1, EOF2 and EOF3, which were previously multiplied with the standard deviations of the corresponding time components; e) time component of the dominant mode, normalized with its standard deviation; f) time component of the second dominant mode, normalized with its standard deviation; g) time component of the third mode, normalized with its standard deviation; d) superposition of the time components associated with the first three EOFs (PC1+PC2+PC3).

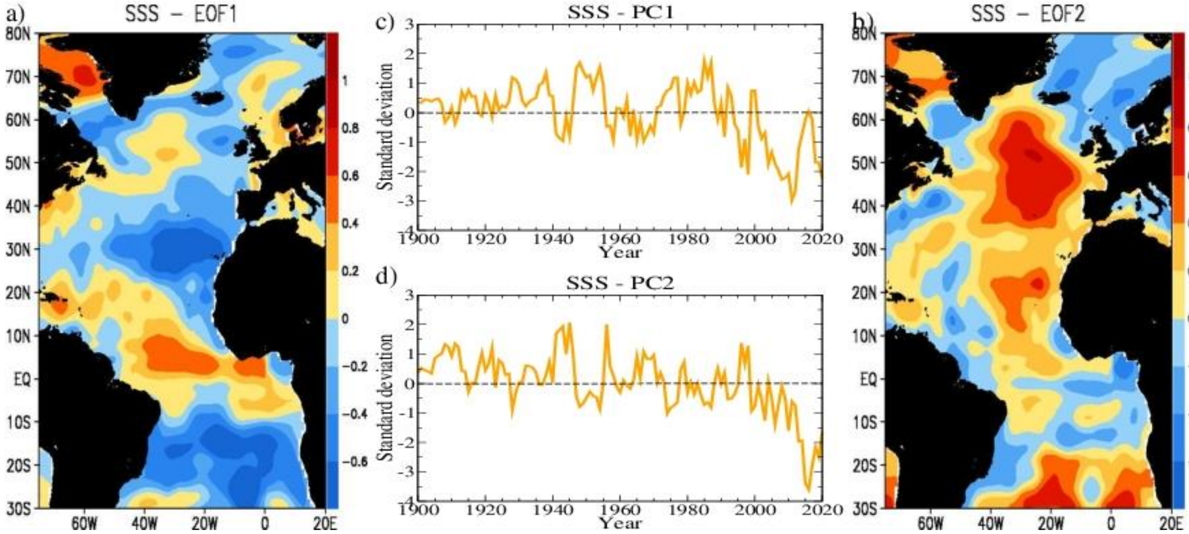

**Supplementary Figure 5 Dominant Atlantic SSS modes** a) EOF1, explaining 11% of variance; b) the associated time component; c) EOF2, explaining 10% of variance; d) the corresponding time component.

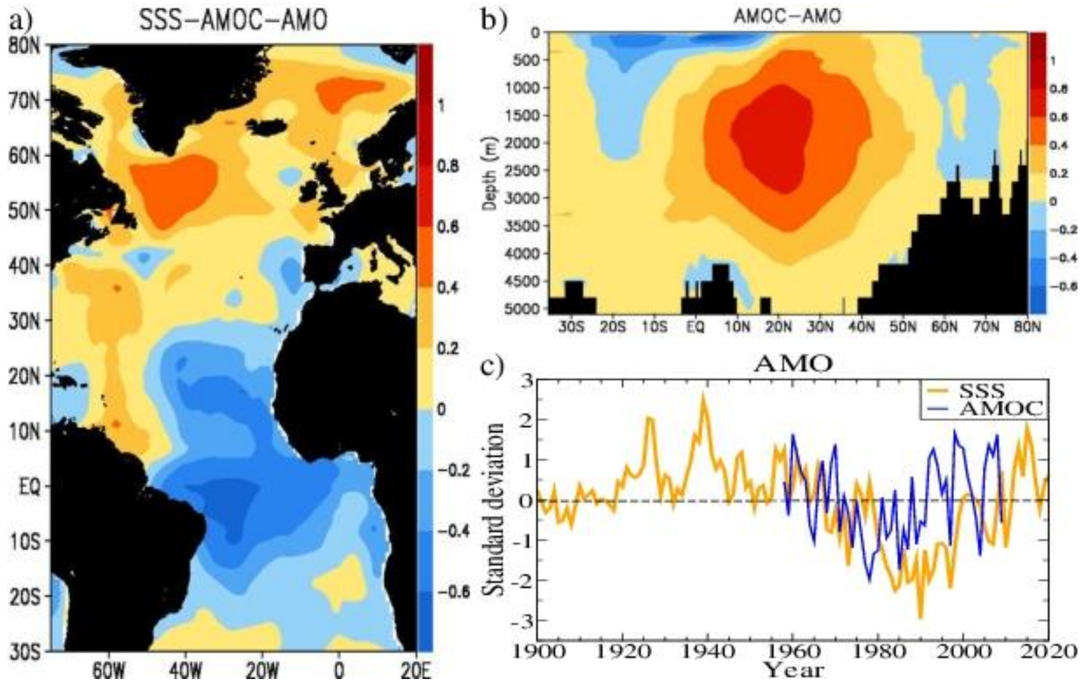


**Supplementary Figure 6 SSS-AMOC-AMO mode** a) Second dominant SSS mode (EOF3) (units less), explaining 7% of variance; b) Second dominant stream function mode (Sv), explaining 21% of variance; c) normalized time components of the second dominant SSS (orange line) and stream function modes (blue line).

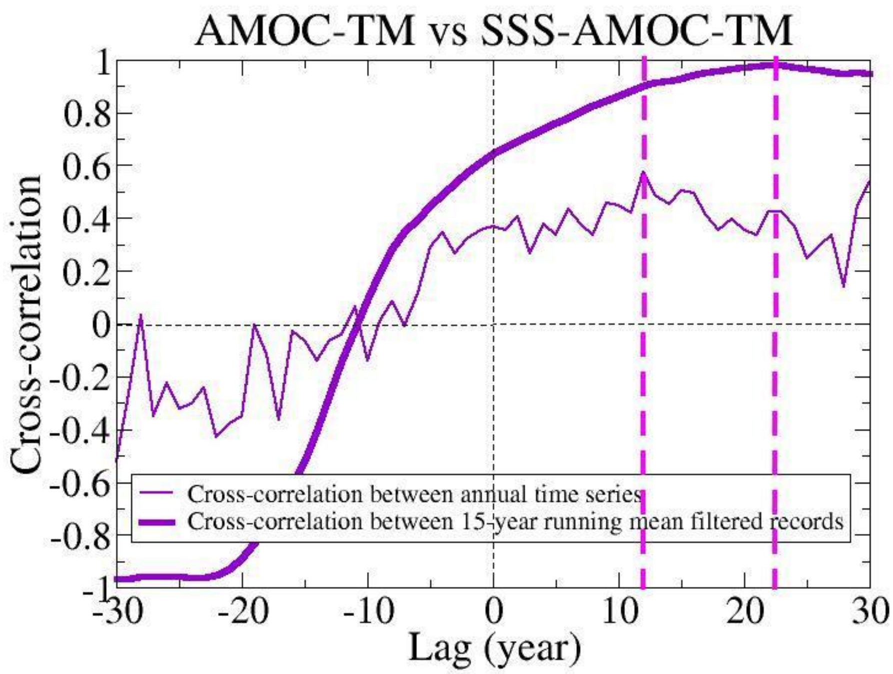


**Supplementary Figure 7 Cross-correlation between the stream-function and SSS time components of the AMOC-Trend Mode** (Fig. 4e). The cross-correlation between the annual (thin violet line) and low-pass (thick violet line) filtered (15 year running mean) records shows maxima when the stream function components leads the SSS time series with 12 and 22 years, respectively.

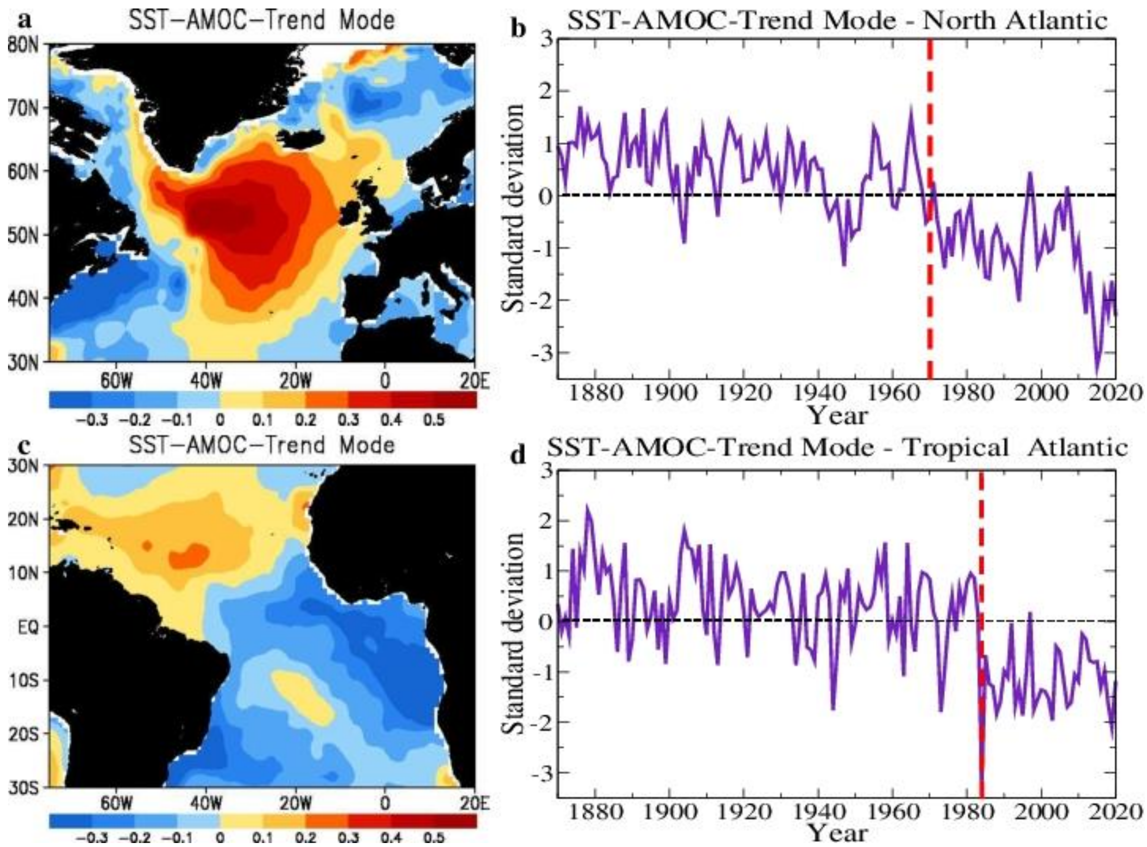


**Supplementary Figure 8 Footprints of the AMOC-TM on the North Atlantic and Tropical Atlantic SST fields**. North Atlantic (a) and Tropical Atlantic (c) SST patterns of the SST-AMOC-TM, derived through EOF analyses over the two sectors, together with the corresponding time components, shown in panels (b) and (d). The vertical red lines mark shifts in the two time series.

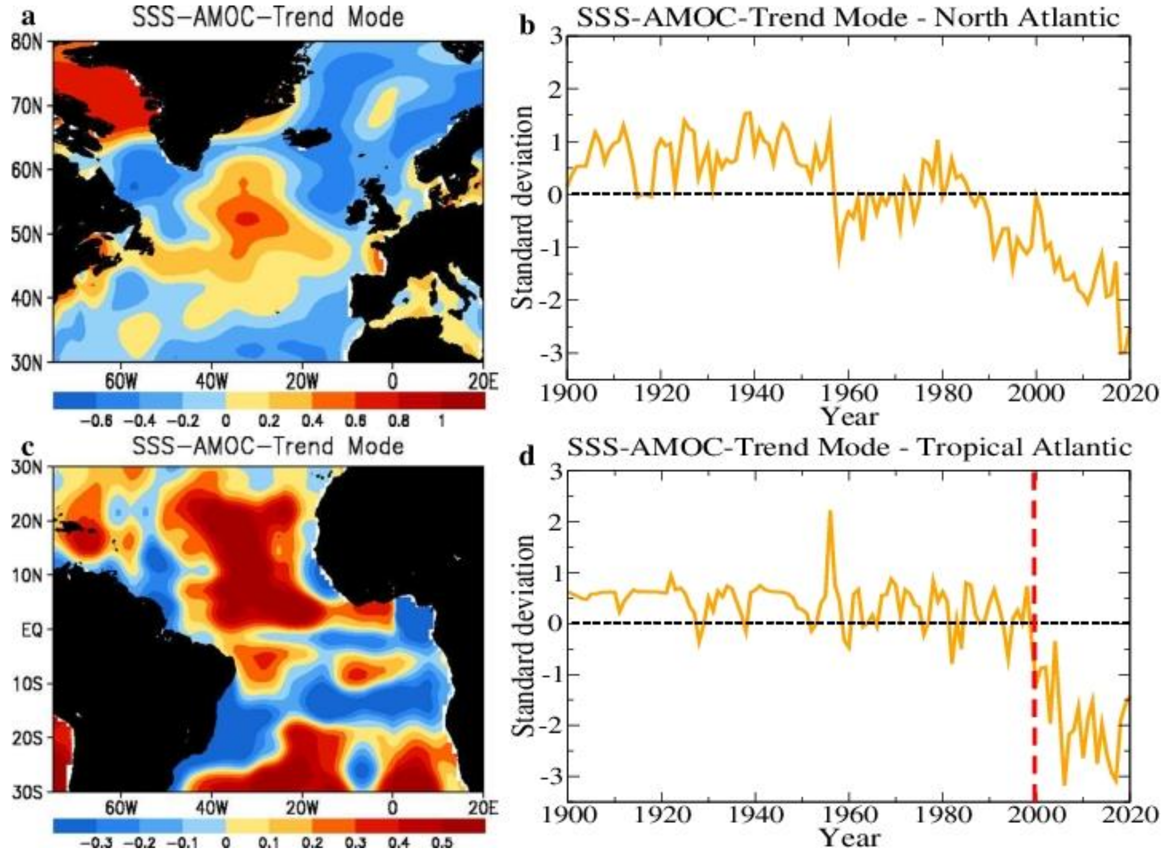


**Supplementary Figure 9 Footprints of the SSS-AMOC-TM on the North Atlantic and Tropical Atlantic SSS fields**. North Atlantic (a) and Tropical Atlantic (c) SSS patterns of the SSS-AMOC-TM, derived through EOF analyses over the two sectors, together with the corresponding time components, shown in panels (b) and (d).

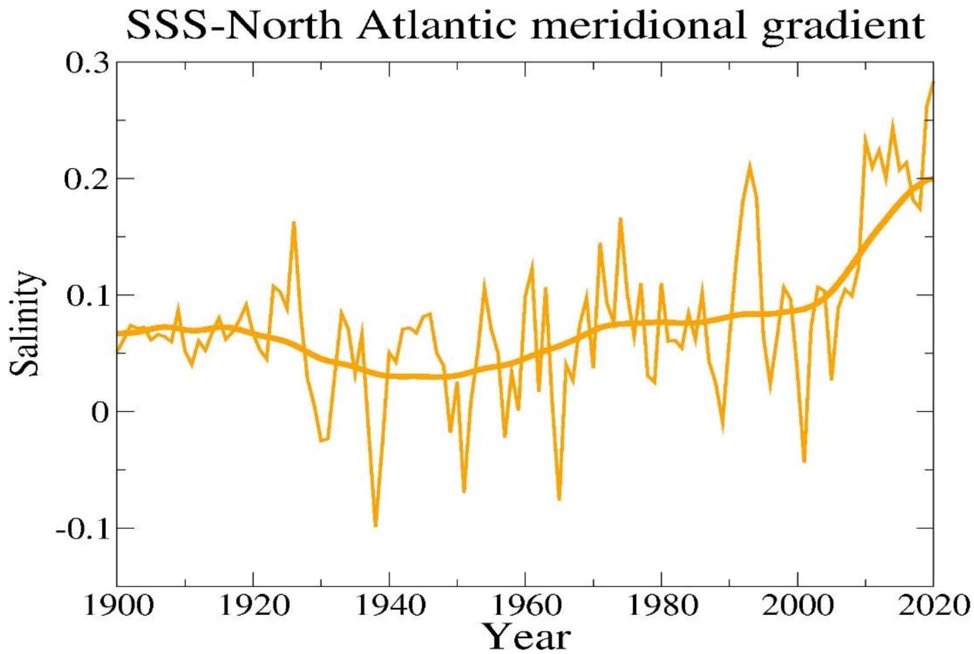


**Supplementary Figure 10 North Atlantic SSS gradient.** The annual SSS gradient time series (thin line) is obtained as the difference between the subtropical and subpolar SSS time series (Fig. 5a). The long-term component of the gradient (thick line) line was reconstructed from the first three components identified through SSA of the annual record, using a 50-year window length.

## 1. Isolating climate modes using the EOF method

A climate mode could be defined as a set of coherent processes associated with distinct spatial and/or temporal patterns. The Empirical Orthogonal Functions (EOF) method decomposes the multidimensional input field in a series of mathematically orthogonal spatial patterns (EOFs), which constitute a new base in which the initial field is represented. By projecting the EOFS on the initial field one obtains their associated time components.

The orthogonality of the patterns is sometimes transferred to the inference that two EOFs are implicitly associated with different climate modes However, two EOFs with distinct structures could be associated with the same climate mode, as it is suggested by a particular example. Let consider an oscillatory mode which is characterized by a specific pattern in its positive phases and by the same structure, but with reverse sign, in its negative phases. Let assume that this pattern is provided by EOF1. The associated time component will reflect the changes in amplitude and sign of the mode's extreme phases. However, during the transition phase between its two extreme states, the mode can manifest through a distinct structure than that specific for its positive and negative manifestations, which is thus not reflected by EOF1. This is possible, for example, for variables related to the ocean state, as this medium has a relatively large memory, which can contribute to the development of different coherent spatial structures. Such a description of the transition/intermediate stages of the same mode could be provided, for example, by the EOF2 spatial pattern. Therefore, although EOF1 and EOF2 have different spatial structures and are orthogonal (in a mathematical sense), they describe different phases and types of manifestation of the same climate mode. One indication that two EOFs could be linked with the same mode is that their time components show similar temporal properties (e.g. both show by multidecadal variations, but shifted in time). In such a case, the time series associated with EOF1 and EOF2 would be correlated for a specific delay between them, reflecting the fact that the two EOFs are describing different phases of the same mode. Least but not last, the consistency and understanding of the physical processes describing the physical processes associated with the two EOFs, validates their association with the same mode.

As another specific example, the El Niño Southern Oscillation (ENSO) phenomenon, the main source of interannual variability at global scale, a complex phenomenon originating in Tropical Pacific, was linked with at least two modes of ENSO manifestation in the SST field: the conventional pattern (also known as Eastern Pacific ENSO) with maximum amplitudes in Eastern Tropical Pacific and the El Niño Modoki (also known as Central Pacific ENSO) (Ashok et al. 2007; Cai et al. 2018). Although the conventional ENSO and El Niño Modoki are associated with different EOFs, they reflect manifestations of the same phenomenon. Furthermore, given that the EOFs constitute a base, it is natural to express a climate mode as a linear combination of eigenvectors.

In synthesis, we argue that two or more EOFs can be associated with the same climate mode, providing a more complete and consistent description of it as would do only one eigenvector, as was described, for example, in a previous study (Dima et al. 2022). Here we consider extensively the possibility that two or more EOFs describe the same mode.

## References

Ashok, K., Behera, S. K., Suryachandra, A. R., Weng, H., Yamagata, T. El Niño Modoki and its possible teleconnections, *J. Geophys. Res. Oceans*, **112**(C11), doi:10.1029/2006JC003798, (2007).

Cai, W., Wang, G., Dewitte, B. *et al.* Increased variability of eastern Pacific El Niño under greenhouse warming. *Nature* **564**, 201–206 (2018).